Adsorption (2006) 12:293–308
DOI 10.1007/s10450-006-0560-2

Adsorption and structural properties of channel-like and cage-like organosilicas

Rafal M. Grudzien · Bogna E. Grabicka · Mietek Jaroniec

Abstract Channel-like and cage-like mesoporous silicas, SBA-15 (*P6mm* symmetry group) and SBA-16 (*Im3m* symmetry group), were modified by introducing single ureidopropyl surface groups, mixed ureidopropyl and mercaptopropyl surface groups, and single bis(propyl)disulfide bridging groups. These hexagonal and cubic organosilicas were prepared under acidic conditions via co-condensation of tetraethyl orthosilicate (TEOS) and proper organosilanes using poly(ethylene oxide)-*block*-poly(propylene oxide)-*block*-poly(ethylene oxide) amphiphilic block copolymer templates, P123 ($EO_{20}PO_{70}EO_{20}$) and F127 ($EO_{106}PO_{70}EO_{106}$). The modified SBA-15 and SBA-16 materials were synthesized by varying the molar ratio of organosilane to TEOS in the initial synthesis gel. The removal of polymeric templates, P123 and F127, was performed with ethanol/hydrochloric acid solution. In the case of SBA-15 the P123 template was fully extracted, whereas this extraction process was less efficient for the removal of F127 template from the SBA-16-type organosilicas; in the latter case a small residue of F127 was retained. The adsorption and structural properties of the resulting materials were studied by nitrogen adsorption-desorption isotherms at -196°C (surface area, pore size distribution, pore volumes), powder X-Ray diffraction, CHNS elemental analysis and high-resolution thermogravimetry. The structural ordering, the BET specific surface area, pore volume and pore size decreased for both channel-like and cage-like mesoporous organosilicas with increasing concentration of incorporated organic groups.

Keywords Channel-like mesostructures · Cage-like mesostructures · Ordered mesoporous organosilicas · Nitrogen adsorption · SBA-15 · SBA-16 · Co-condensation synthesis · Ureidopropyl surface group · Mercaptopropyl surface group · Bis(propyl)disulfide bridging group

R. M. Grudzien · B. E. Grabicka · M. Jaroniec (✉)
Department of Chemistry, Kent State University, Kent, Ohio 44242, USA
e-mail: jaroniec@kent.edu

1 Introduction

The discovery of ordered mesoporous silicas (OMSs) (Kresge et al., 1992; Beck et al., 1992; Yanagisawa et al., 1990) has attracted a lot of worldwide attention because of their potential applications as catalysts, adsorbents and advanced materials for nanotechnology. Initially, OMSs were synthesized via self-assembly process driven by electrostatic interactions between the anionic silica species and cationic alkyltrimethylammonium surfactants possessing from eight to twenty two carbon atoms in the alkyl chain used as structure directing agents (Kresge et al., 1992). This synthesis led to the formation of ordered silica, known as MCM-41 (Kresge et al., 1992; Beck et al., 1992), consisting of two-dimensional hexagonal arrangement

of cylindrical channels (*P6mm*) with controllable pore size in the range from 2 to 7 nm (Kruk et al., 2000).

A few years later Zhao and co-workers (1998) contributed meaningfully to the field of OMSs by developing a new synthetic strategy that allowed expanding the mesopore size of OMSs for several nanometers. The key element of this synthesis was the use of inexpensive nonionic block copolymers that can be easily recycled and recovered instead of environmentally unfriendly ionic surfactants (Zhao et al., 1998; Abu-Lebdeh et al., 1998). Their investigation led to the discovery of a very prominent OMS, namely SBA-15 (Zhao et al., 1998), which is a two dimensional hexagonal structure (*P6mm*) of cylindrical channel-like mesopores interconnected through disordered smaller complementary pores (Kruk et al., 2000). SBA-15 has been synthesized under strong acidic conditions by employing amphiphilic poly(ethylene oxide)-*block*-poly(propylene oxide)-*block*-poly(ethylene oxide) triblock copolymer P123 ($EO_{20}PO_{70}EO_{20}$) via controlled hydrolysis and condensation of tetraethyl orthosilicate (TEOS) followed by removal of polymeric template by either extraction with ethanol and acid or calcination at elevated temperatures (Zhao et al., 1998; Kruk et al., 2000; Yang et al., 1999; Zhang et al., 2005). SBA-15 differs from MCM-41 not only because of larger mesopores and irregular interconnections but also because of higher hydrothermal and thermal stability caused by its thicker mesopore walls (Yang et al., 1999; Zhang et al., 2005).

Further developments in the area of OMSs gave rise to another important member of polymer-templated OMS with a 3-dimensional cubic (*Im3m*) arrangement of cage-like mesopores (Sakamoto et al., 2000), in which each cage is connected with eight neighboring cages via small apertures (Zhao et al., 1998). This large-pore and thick-wall material (Zhao et al., 1998; Voort et al., 2002; Wang et al., 2004; Kim et al., 2004; Grudzien et al., 2006; Gierszal et al., 2005) was prepared by employing commercial triblock copolymer F127 ($EO_{106}PO_{70}EO_{106}$), which possesses the same number of hydrophobic poly(propylene oxide) (PPO) blocks and much larger number of hydrophilic poly(ethylene oxide) (PEO) blocks than P123 (106 instead of 20 in the latter). However, increasing the hydrophobicity of core blocks in the polymeric template by replacing PPO blocks with poly(butylene oxide) (PBO) led to the development of a cubic OMS with even higher curvature. When poly(ethylene oxide)-*block*-poly(butylene oxide)-*block*-poly(ethylene oxide) triblock copolymer B50-6600 ($EO_{39}BO_{47}EO_{39}$) (Yu et al., 2000) was used as a soft template a three dimensional cubic (*Fm3m*) OMS, FDU-1, was obtained (Kruk et al., 2002; Matos et al., 2003). FDU-1 exhibits even larger cage-like mesopores than its cubic counterpart SBA-16 (Zhao et al., 1998) and four more connections (totally twelve) with neighboring cages (Yu et al., 2000; Kruk et al., 2002; Grudzien and Jaroniec, 2005; Grudzien et al., 2006). In general, an extraordinary stability of 3-dimensional SBA-16 (Zhao et al., 1998) and FDU-1 (Kruk et al., 2004) silicas exhibiting large cage-like mesopores and much smaller connecting apertures could be advantageous for diffusion of molecules as well as selective adsorption and catalysis due to their smaller susceptibility for pore blockage.

The diversity of mesoporous sieves (Kresge et al., 1992; Yanagisawa et al., 1990; Zhao et al., 1998; Yu et al., 2000) has been extended by constructing new hybrid inorganic materials, referred as ordered mesoporous organosilicas (OMOs), which feature decorated mesopore walls and highly accessible organic groups (Beck et al., 1992; Jaroniec, 2006). The introduction of proper functionalities to OMSs is a convenient way for the creation of OMOs with the desired optical, mechanical and electrical properties, which make them attractive materials for catalytic and adsorption processes, sensing devices and environmental applications (Antochshuk et al., 2003; Olkhovyk et al., 2004; Olkhovyk and Jaroniec, 2005). The synthesis of OMOs can be done via two major routes: (i) by post-synthesis modification of the template-free mesoporous silica with appropriate organosilane (Beck et al., 1992; Feng et al., 1997; Lim et al., 1997; Jaroniec et al., 1998; Lim and Stein, 1999; Antochshuk and Jaroniec, 1999; Kang et al., 2004; Srivastava et al., 2006; Zapilko and Anwander, 2006) or by post-synthesis modification of the template-containing mesoporous silica with desired organosilane (Antochshuk and Jaroniec, 1999; Antochshuk and Jaroniec, 2000) and by (ii) direct one-pot synthesis, also known as co-condensation synthesis (Kruk et al., 2002; Wang et al., 2003; Kao et al., 2006; Fiorilli et al., 2005; Yang et al., 2004; Wang et al., 2005, Fowler et al., 1997; Gong et al., 2001, Huh et al., 2003; Hodgkins et al., 2005; Wei et al., 2005; Hamoudi and Kaliaguine, 2003). The direct one-pot synthesis in contrast to the post-synthesis grafting is particularly prominent because of its simplicity and efficiency. Furthermore, it affords OMOs with relatively high loadings of functional ligands and large pore diameters

due to the formation of functionalized mesostructure in the presence of micelles and the elimination of calcination procedure that causes the structure shrinkage.

Alternatively, the material's framework can be also functionalized by incorporating organic bridging groups inside the mesopore walls (Melde et al., 1999; Asefa et al., 1999; Inagaki et al., 1999). The resulting materials, known as periodic mesoporous organosilicas (PMOs) are also prepared by co-condensation but using bridged silsesquioxanes $(R' O)_3Si\text{-}R\text{-}Si(OR')_3$ as silica-containing precursors instead of trialkoxyorganosilane $(R'O)_3Si\text{-}R$ as precursors (R is a functional group). Furthermore, the one-pot route has been used to incorporate a variety of bridging spacers including small aliphatic groups (Matos et al., 2002; Bao et al., 2004; Zhao et al., 2004; Liang et al., 2005) like methylene, ethane and ethene as well as large aromatic spacers such as phenylene (Inagaki et al., 2002), thiophene, 1,3,5-benzene ring linked with three silicon atoms (Kuroki et al., 2002), 1,4,8,11-tetraazacyclotetradecane (Corriu et al., 2002) and recently isocyanurate ring integrated with three silyls via flexible propyl chains (Olkhovyk and Jaroniec, 2005; Olkhovyk et al., 2005; Grudzien et al., 2006) (for details see reviews by Stein et al. (2000, 2003) and Hatton et al. (2005) and references therein).

Overall, co-condensation was explored to attach surface groups such as methyl (Kruk et al., 2002), vinyl (Wang et al., 2003; Kao et al., 2006), carboxylic (Fiorilli et al., 2005; Yang et al., 2004), aminopropyl (Wang et al., 2005) and imidazole (Fowler et al., 1997; Grudzien et al., 2006) into the mesopore walls of ordered silicas including mostly channel-like structures such as MCM-41 and SBA-15, and to the less extent, cage-like structures such as SBA-16 and FDU-1.

Gong and co-workers (2001) have studied the incorporation of ureidopropyl ligands into the 3-dimensional wormhole-like porous MSU-X material by one-pot route as well as the synthesis of a bi-functional MSU-X containing ureidopropyl group along with small alkyl and aromatic groups such as methyl and phenyl. Later, Huh and co-workers (2003) have reported co-condensation synthesis of ureidopropyl-functionalized MCM-41 silicas templated by cetyltrimethylammonium bromide (CTAB) ionic surfactant under basic pH.

Numerous papers have been published on the synthesis of mercaptopropyl-functionalized OMSs (Huh et al., 2003; Hodgkins et al 2005; Wei et al., 2005; Hamoudi and Kaliaguine, 2003) by both post-synthesis grafting and co-condensation routes because of high affinity of this group towards heavy metal ions such as Hg^{2+}, Pb^{2+}, Cd^{2+} and Zn^{2+}. Moreover, thiol-functionalized mesoporous materials were found to be useful in catalysis because of their easiness to the oxidation, which gives sulfonic groups (Hamoudi and Kaliaguine, 2003). There are many reported organosilicas with thiol surface groups for both hexagonal and cubic symmetries.

Zhang and co-workers (2003) reported a thioether-functionalized mesoporous silica via co-condensation of TEOS and (1,4)-bis(triethoxysilyl)propane tetrasulfide in the presence of Pluronic P123. Zhang et al. showed that the aforementioned PMO, containing thioether spacers, selectively binds Hg^{2+} ions. More recently, Liu at al. (2005) incorporated the same thioether to MCM-41 and showed its high adsorption affinity to Hg^{2+} as well as for organic pollutants such as phenols.

In particular, a lot of research has been devoted to decorate the surfactant-templated MSU, HMS (Tanev et al., 1994; Tanev and Pinnavaia, 1995) and MCM-41 as well as polymer-templated SBA-15 and SBA-16 silicas. However, to the best of our knowledge, there is no report on bi-functional SBA-15 and SBA-16 OMSs with mercaptopropyl and ureidopropyl surface groups as well as thioether-functionalized SBA-15 and SBA-16 materials containing disulfide bridging groups.

The main goal of the present work is to take advantage of co-condensation method to decorate the internal surface of channel-like and cage-like mesoporous silicas SBA-15 (P6mm) and SBA-16 (Im3m) with single ureidopropyl surface groups and mixed functionality consisting of ureidopropyl and mercaptopropyl surface groups as well as to design the framework with bridging bis(propyl)disulfide groups. Furthermore, the objective of this work is to perform a comparative study how adsorption properties such as the specific surface area, pore size and pore volumes and structural properties such as the unit cell and the size of pore openings change with gradual incorporation of organic functional groups into their hexagonal and cubic structures.

2 Experimental

2.1 Chemicals

Structure directing agents: triblock copolymers Pluronic P123 ($EO_{20}PO_{70}EO_{20}$) and Pluronic F127

($EO_{106}PO_{70}EO_{106}$) were purchased from BASF Corporation. Silica source: tetraethyl orthosilicate (TEOS) was received from Across Organics (98%), whereas other organosilanes: ureidopropyltrimethoxysilane and 3-mercaptopropylsilane and bis(triethoxysilylpropyl) disulfide (90%) were obtained from Gelest, Inc. Deionized water (DW; resistivity $< 17.5\,M\Omega cm$) was obtained using in-house Ionpure Plus 150 Service Deionization ion-exchange purification system. All chemicals were used as received without further purification.

2.2 Syntheses of mesoporous channel-like SBA-15 organosilicas

Syntheses of all channel-like mesoporous SBA-15 silicas were performed in the presence of poly (ethylene oxide)-*block*-poly(propylene oxide)-*block*-poly(ethylene oxide) triblock copolymer (P123, $EO_{20}PO_{70}EO_{20}$) by co-condensation of tetraethyl orthosilicate (TEOS) and either trialkoxyorganosilanes $(R/O)_3Si\text{-}R$ (where R denotes functional group) or bridged silsesquioxane $(R'O)_3Si\text{-}R\text{-}Si(OR')_3$ to introduce the desired surface and framework functionalities, respectively. In general, ureidopropyl-functionalized SBA-15 materials were synthesized by one-pot route using ureidopropyltrimethoxysilane (U) and TEOS, bifunctional SBA-15 containing ureidopropyl and mercaptopropyl surface groups were prepared using ureidopropyltrimethoxysilane, 3-mercaptopropylsilane and TEOS, whereas the framework-modified SBA-15 was obtained by using bis(triethoxysilylpropyl) disulfide and TEOS (see Scheme 1 and 2). The adopted procedure was similar to that used for the synthesis of SBA-15 reported elsewhere (Zhao et al., 1998). In a typical synthesis, 2 g of polymer was dissolved in 61.2 ml of 2M HCl and 10.8 ml of deionized water (DW) under vigorous stirring at 40°C. After 4–6 h of stirring a specified volume of TEOS was added dropwise to this solution under vigorous mixing, and then after 15 minutes organosilane was pipetted to achieve the desired molar composition of both silanes (see Table 1). The resulting mixture was stirred for 24 h followed by aging at 100°C for 48 h. The white solid was washed with DW, filtered and dried at 80°C. The template was removed by extraction three times with 2 ml of 36 wt.% HCl and 100 ml of 95% ethanol at 70°C. The extracted ureidopropyl-functionalized SBA-15, ureidopropyl-mercaptopropyl-functionalized SBA-15 and framework-functionalized SBA-15 samples are denoted as SBA-15-Ux, SBA-15-U1-SHy and SBA-15-DSz, where U, SH and DS refer to ureidopropyl and

Table 1 Molar composition for the synthesis gels used and the corresponding elemental analysis data for the organic-functionalized channel-like SBA-15 mesoporous silicas[a]

	Synthesis gel composition						Elemental analysis			
	n, (mmoles)				*P*, (%)		*C*, (mmoles/g)		*P*, (%)	
Sample	TEOS	U	SH	DS	P_N	P_S	C_U	C_{SH} or C_{DS}	P_N	P_S
SBA-15	19.20									
SBA-15-U1	18.24	0.96			2.16		0.43		1.2	
SBA-15-U2	17.28	1.92			4.04		0.79		2.2	
SBA-15-U3	16.32	2.88			5.67		1.27		3.5	
SBA-15-U4	15.36	3.84			7.12		0.92		2.5	
SBA-15-U1-SH1	17.76	0.96	0.48		2.11	1.21	0.37	0.26	1.0	0.83
SBA-15-U1-SH2	16.80	0.96	1.44		2.01	3.45	0.26	0.81	0.7	2.60
SBA-15-DS1	18.72			0.24		1.30		0.31		1.99
SBA-15-DS2	17.76			0.72		3.70		0.49		3.16
SBA-15-DS3	17.28			0.96		4.81		0.46		2.69
SBA-15-DS4	16.32			1.44		6.89		0.96		6.15

[a]*n*TEOS, number of mmoles of tetraethyl orthosilicate; *n*U, number of mmoles of ureidopropyltrimethoxysilane; *n*SH, number of mmoles of 3-mercaptopropylsilane; *n*DS, number of mmoles of bis(triethoxysilylpropyl) disulfide, P_N and P_S, nitrogen and sulfur percentages predicted on the basis of the synthesis gel mixture; C_U, C_{SH} or C_{DS} concentration of functional groups in the resulting materials calculated on the basis of nitrogen or sulfur percentages obtained by elemental analysis; P_N and P_S, nitrogen and sulfur weight percentages obtained from elemental analysis.

Table 2 Molar composition for the synthesis gels used and the corresponding elemental analysis data for the organic-functionalized cage-like SBA-16 mesoporous silicas[a]

	Synthesis gel composition						Elemental analysis			
	n, (mmoles)				*P*, (%)		*C*, (mmoles/g)		*P*, (%)	
Sample	TEOS	U	SH	DS	P_N	P_S	C_U	C_{SH} or C_{DS}	P_N	P_S
SBA-16	20.16									
SBA-16-U1	19.15	1.01			2.17		0.91		2.5	
SBA-16-U2	18.14	2.02			4.04		0.92		2.5	
SBA-16-U3	17.14	3.02			5.67		1.11		3.1	
SBA-16-U1-SH1	18.14	1.01	1.01		2.06	2.36	0.40	0.69	1.1	2.21
SBA-16-U1-SH2	17.14	1.01	2.02		1.96	4.49	0.39	1.32	1.0	4.23
SBA-16-U1-SH3	16.13	1.01	3.02		1.88	6.42	0.42	1.67	1.1	5.35
SBA-16-DS1	19.66			0.5		2.45		0.45		2.92
SBA-16-DS2	18.65			1.01		4.72		0.83		5.31
SBA-16-DS3	18.14			2.02		8.12		0.98		6.26

[a]*n*TEOS, number of mmoles of tetraethyl orthosilicate; *n*U, number of mmoles of ureidopropyltrimethoxysilane; *n*SH, number of mmoles of 3-mercaptopropylsilane; *n*DS, number of mmoles of bis(triethoxysilylpropyl) disulfide, P_N and P_S, nitrogen and sulfur percentages predicted on the basis of the synthesis gel mixture; C_U, C_{SH} or C_{DS} concentration of functional groups in the resulting materials calculated on the basis of nitrogen or sulfur percentages obtained by elemental analysis; P_N and P_S, nitrogen and sulfur weight percentages obtained from elemental analysis.

mercaptopropyl surface groups and bridging disulfide groups, respectively. Letters *x, y* and $z = 1, 2, 3, 4$ refer to the samples with successively growing concentration of functional groups (see Table 1). The letter *t* refers to the as-synthesized organic-functionalized silica. The pure channel-like silica subjected to calcination at 550°C in flowing air for 4 hours was denoted as SBA-15.

2.3 Syntheses of mesoporous cage-like SBA-16 organosilicas

Cage-like mesoporous SBA-16 silicas with functional surface and bridging groups (see Scheme 1 and 3) were synthesized similarly to SBA-15 by co-condensation of TEOS and proper organosilanes in the presence of poly(ethylene oxide)-*block*-poly(propylene oxide)-*block*-poly(ethylene oxide) triblock copolymer (Pluronic F127, $EO_{106}PO_{70}EO_{106}$). The procedure adopted is a slightly modified recipe reported by Qiu et al. (2004). In a typical synthesis, 1 g of F127 and 3.527 g of sodium chloride were dissolved in 10 ml 2 M HCl and 30 ml deionized water at 40°C. After 4 hours stirring a specified volume of TEOS was pipetted drop wise to this solution under vigorous mixing, and next after 15 minutes organosilane was added to achieve the desired molar composition of both silanes (see Table 2). After further stirring for 20 h at 40°C, the resulting white precipitate was transferred into a polypropylene bottle and subsequently heated at 100°C for 24 h . The product was filtered, washed with DW, and dried in the oven at 80°C. To remove the polymeric template from mesopores, the as-synthesized nanocomposites were extracted three times with 2 ml of 36 wt.% HCl and 100 ml of 95% ethanol at 70°C. The extracted ureidopropyl-functionalized

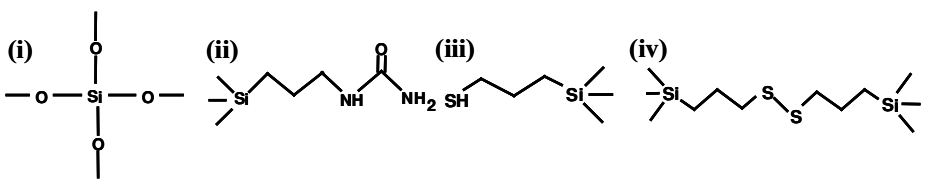

Scheme 1 Chemical structures of (i) tetraethyl orthosilicate (TEOS, silica source) and (ii–iv) functional silanes used in polymer-templated co-condensation synthesis involving (ii) ureidopropyltrimethoxysilane and (iii) 3-mercaptopropylsilane as well as (iv) bis(triethoxysilylpropyl) disulfide

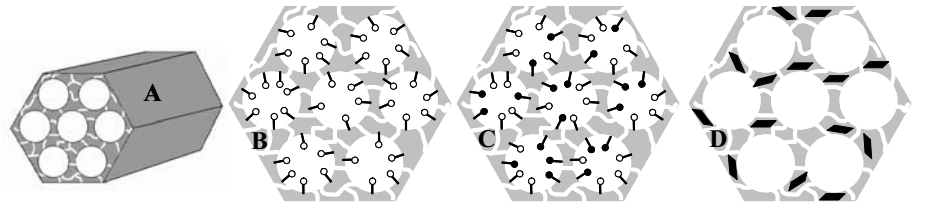

Scheme 2 Schematic illustration of mesoporous channel-like structure SBA-15 silica (A) and interconnected cylindrical channels (large circle with thin channels) containing ureidopropyl surface ligands (B) (open circles), bifunctional ureidopropyl (open circles), as well as mercaptopropyl (filled circles) surface ligands (C), and bis(propyl)disulfide bridging groups (D) (filled rhombus)

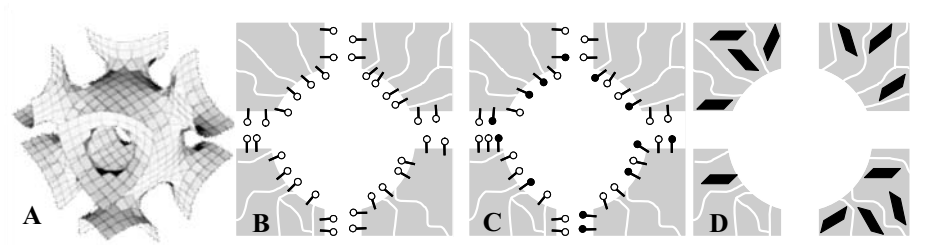

Scheme 3 Schematic illustration of mesoporous cage-like structure SBA-16 silica (A) and interconnected spherical cages (large circle with straight channels) containing ureidopropyl surface ligands (B) (open circles), bifunctional ureidopropyl (open circles) as well as mercaptopropyl (filled circles) surface ligands (C) and bis(propyl)disulfide bridging groups (D) (filled rhombus)

SBA-16, ureidopropyl-mercaptopropyl-functionalized SBA-16 and framework-functionalized SBA-16 samples are denoted as SBA-16-Ux, SBA-16-U1-SHy and SBA-16-DSz, where U, SH and DS refers to ureidopropyl and mercaptopropyl surface groups as well as to the bridging disulfide groups, respectively. Letters *x, y* and $z = 1, 2, 3$ refer to the samples with successively growing concentration of functional groups (see Table 2). The letter *t* refers to as-synthesized sample, i.e., sample containing polymeric template. The pure silica sample subjected to calcination at 550°C in flowing air for 4 h was denoted as SBA-16.

2.4 Measurements

Nitrogen adsorption measurements were performed using ASAP 2010 and ASAP 2020 volumetric analyzers manufactured by Micromeritics, Inc. (Norcross, GA). Adsorption isotherms were measured at −196°C over the interval of relative pressures from 10^{-6} to 0.995 using high purity nitrogen of 99.998% from Praxair Distribution Company (Canton, OH, USA), which was used to measure the amount adsorbed as a function of the equilibrium pressure. Prior to each adsorption measurement the pure and functionalized silicas were outgassed under vacuum in the port of the adsorption instrument for at least 2 h at 200°C and 110°C, respectively until the residual pressure dropped to 6 or less μmHg. Such temperature was chosen on the basis of thermogravimetric analysis to avoid the degradation of surface ligands and to remove adsorbed gases, ethanol and water.

Quantitative estimation of organic groups was performed by carbon, hydrogen, nitrogen and sulphur (CHNS) analysis. Nitrogen and sulfur contents for all organosilicas were determined using a LECO model CHNS-932 elemental analyzer from St. Joseph, MI. The surface coverage of functional groups expressed per gram of the entire sample was calculated from nitrogen and sulfur contents obtained from elemental analysis.

Thermogravimetric analysis was carried out under nitrogen atmosphere using a TA Instruments Inc. (New Castle, DE, USA) model TGA 2950 high-resolution thermogravimetric analyzer. The weight change (TG) patterns were recorded over a temperature range from 35°C to 800°C. The instrument was equipped with an open platinum pan and an automatically programmed temperature controller. The high-resolution mode was used to record the TG data. The heating rate was

adjusted automatically during measurements to achieve the best resolution; its maximum was 5°C min^{-1}. The resolution and sensitivity parameters were 4 and 6, respectively. The flow rate of nitrogen gas in the system was 100 and 60 cm^3 min^{-1} on the furnace and balance, respectively.

Powder X-ray diffraction (XRD) measurements were recorded using a PANanalytical, Inc. X'Pert Pro (MPD) Multi Purpose Diffractometer with Cu Kα radiation, operating voltage of 40 kV, 0.01° step size and 20 s step time over a range $0.5^\circ < 2\theta < 3.0^\circ$ at room temperature.

2.5 Calculations

The specific surface area (S_{BET}, m^2/g) for the samples under study was calculated by employing the Brunauer-Emmett-Teller (BET) method (Brunauer et al., 1938) in the range of relative pressures from 0.05 to 0.2 (Sing et al., 1985). The volume of complementary pores for the SBA-15 and SBA-16 silicas was calculated by integration the pore size distribution (PSD) up to 4 nm; this integration limit was established on the basis of the first peak of the distribution function representing complementary pores. This volume denoted as V_c (cm^3/g) includes the volume of irregular micropores present in the mesopore walls as well as small apertures that connect ordered cage-like mesopores. The single-point total pore volume (V_t, cm^3/g) (Sing et al., 1985) was estimated from the amount adsorbed at a relative pressure p/p_o of 0.99, where p and p_o denote the equilibrium pressure and saturation vapor pressure, respectively. The pore size distribution was calculated from the adsorption branch of nitrogen adsorption isotherms by using the KJS (Kruk, Jaroniec and Sayari) method (Kruk et al., 1997). This method employs the BJH (Barrett, Joyner and Halenda) algorithm (Barrett et al., 1951) with a relation between the pore size and capillary condensation pressure derived on the basis of adsorption data for high-quality MCM-41 materials with cylindrical pores. The primary mesopore diameter (w_{KJS}, nm) was defined at the maximum of PSD. Since, the PSD analysis was done under assumption of cylindrical pore geometry, while cage-like mesopores are rather spherical, this method leads to a systematic underestimation of the size of mesopore cages by approximately 2 nm (Kruk et al., 2002; Matos et al., 2003). Therefore, the primary mesopore diameters were also evaluated by using proper geometrical relations between the pore size (w_d, nm), volume of complementary pores (V_c, cm^3/g), volume of primary mesopores (V_p, cm^3/g) and unit cell (a, nm) derived for the *Im3m* (Eq. (1)) (Kruk and Jaroniec, 2002) and *P6mm* (Eq. (2)) (Kruk et al., 1999) symmetry groups, respectively.

$$w_d = 0.985 \cdot a \cdot \left(\frac{V_p}{1/\rho + V_c + V_p} \right)^{1/3} \quad (1)$$

$$w_d = 1.05 \cdot a \cdot \left(\frac{V_p}{1/\rho + V_c + V_p} \right)^{1/2} \quad (2)$$

where the symbol ρ denotes the organosilica density, which was assumed to be 2.0 g/cm^3. It is noteworthy that the pure amorphous silica density is 2.2 g/cm^3. The pore wall thickness (b, nm) for *Im3m* and *P6mm* symmetries was assessed by using the following equations 3 and 4, respectively.

$$b = (a\sqrt{3}/2 - w_d) \quad (3)$$

$$b = (a - w_d) \quad (4)$$

The unit-cell parameter (a, nm) for SBA-16 (Eq. (5)) and SBA-15 (Eq. (6)) was evaluated using the interplanar spacing (d, nm) corresponding to (110) and (100) peaks, respectively, on the powder XRD pattern.

$$a = d_{110} \cdot \sqrt{2} \quad (5)$$

$$a = d_{100} \cdot 2 \cdot 3^{-1/2} \quad (6)$$

3 Results and discussion

3.1 Mesoporous channel-like SBA-15 organosilicas

The amounts of ureidopropyl surface groups in SBA-15 with single organic functionality, ureidopropyl and mercaptopropyl surface groups in bi-functional SBA-15 as well as bridging disulfide spacers in SBA-15 were estimated on the basis of elemental analysis data (see Table 1). The nitrogen and sulfur contents obtained for the resulting OMOs by elemental analysis represent around 50–85% of the values estimated on the basis of the initial molar composition of the synthesis gel mixture, indicating quite good incorporation efficiency.

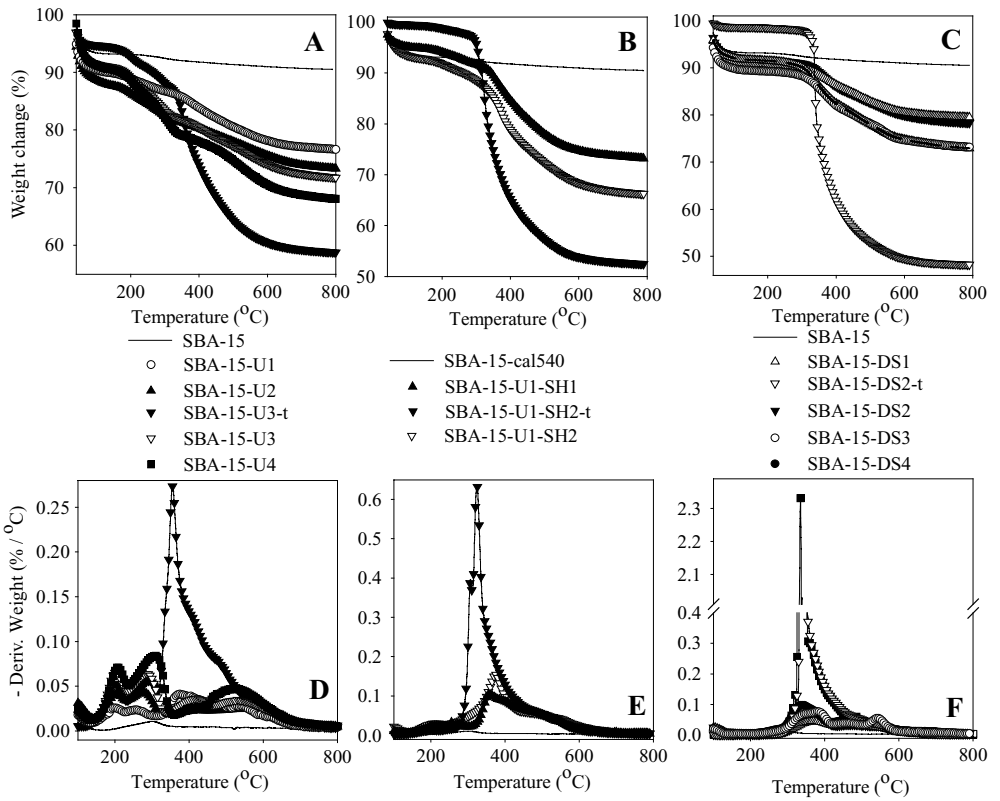

Fig. 1 High-resolution TG profiles (top panels) and the corresponding DTG profiles (bottom panels) recorded in flowing nitrogen for channel-like SBA-15 mesoporous silicas obtained via co-condensation route using various concentrations of ureidopropyl (U) surface ligands (A, D), bifunctional surface ligands: ureidopropyl (U) and mercaptopropyl (SH) (B, E) and bis(propyl)disulfide (DS) bridging groups (C, F), respectively

The introduction of organics into channel-like SBA-15 mesostructure was monitored by high-resolution thermogravimetry (TG). The TG patterns and the corresponding differential TG (DTG) profiles for ureidopropyl-functionalized SBA-15 silicas (Panels A and D), ureidopropyl-mercaptopropyl-functionalized SBA-15 silicas (Panels B and E) and bis(propyl)disulfide-modified SBA-15 (Panels C and F) recorded under nitrogen atmosphere are displayed in Fig. 1, respectively. It is noteworthy that each panel for both TG and DTG curves in Fig. 1 shows profiles for the template-containing organosilicas (their codes contain symbol *t*); see the DTG curves for SBA-15-U3-*t*, SBA-15-U1-SH2-*t* and SBA-15-DS2-*t* shown in Panels A, B and C. As can be seen from these figures the ranges of the TG patterns below 100°C and above 500°C reflect thermodesorption of physisorbed water and ethanol as well as the condensation of silanol groups and decomposition of some residual organic groups, respectively. The range between the aforementioned regions reflects the template removal and decomposition of incorporated organic groups. A complete removal of P123 has been achieved by extraction process with hydrochloric acid and ethanol solution at 80°C as confirmed by the disappearance of the major peak (see the DTG curve for the extracted SBA-15-U3 sample), while the ureidopropyl ligands were remained. Similarly to the ureidopropyl-modified SBA-15 materials the extraction used was also efficient in the case of bi-functional silicas (Panels B and E) and disulfide-containing periodic organosilicas (Panels C and F). The intensity of the minor decomposition peaks observed in the range between 200 and 300°C on the DTG curves for the template-free organosilicas with increasing concentration of ureidopropyl groups (SBA-15-U1, SBA-15-U2, SBA-15-U3 and SBA-15-U4) increases gradually, which indicates that the functionalization was effective.

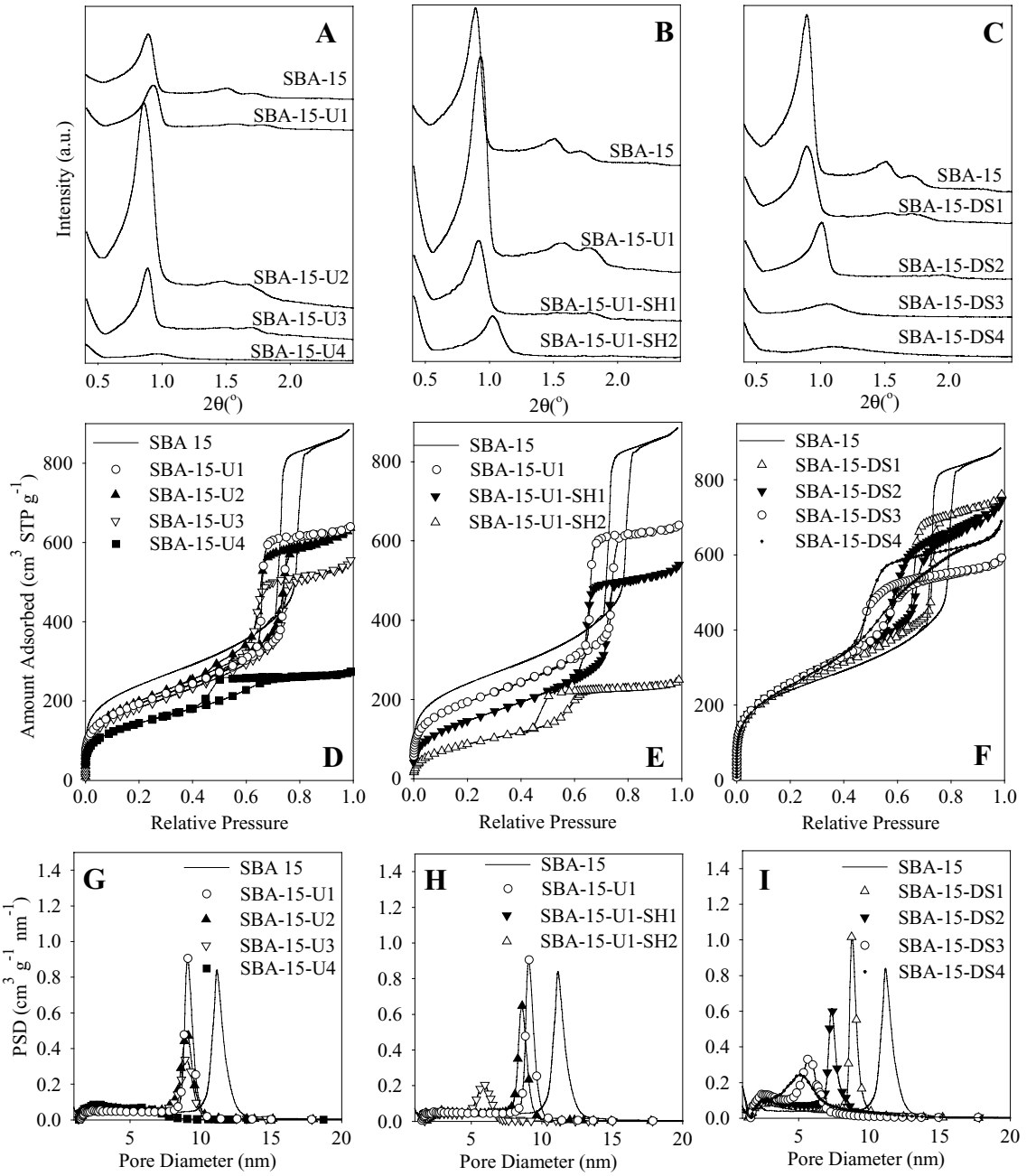

Fig. 2 X-ray diffraction (XRD) patterns (A, B, C), nitrogen adsorption isotherms (D, E, F) measured at –196°C and the corresponding pore size distributions (PSDs) (G, H, I) calculated according to the KJS method (Kruk et al., 1997) for the channel-like SBA-15 mesoporous silicas having various concentrations of ureidopropyl (U) surface ligands (A, D, G), bifunctional surface ligands: ureidopropyl (U) and mercaptopropyl (SH) (B, E, H) and bis(propyl)disulfide (DS) bridging groups (C, F, I), respectively

Structural identification

Structural characterization of the extracted SBA-15 organosilicas containing ureidopropyl surface groups, two different surface groups: ureidopropyl and mercaptopropyl, and bridging bis(propyl)disulfide groups was performed on the basis of the XRD patterns shown in Fig. 2 (Panels A, B and C, respectively).

Table 3 Selected structural parameters of the organic-functionalized channel-like SBA-15 mesoporous silicas[a]

Sample	S_{BET}, m^2g^{-1}	V_t, ccg^{-1}	V_c, ccg^{-1}	w_{KJS}, nm	w_d, nm	b, nm	a, nm
SBA-15	866	1.38	0.13	11.2	9.7	1.8	11.5
SBA-15-U1	702	1.00	0.10	9.1	9.1	2.1	11.2
SBA-15-U2	731	1.00	0.14	9.1	9.5	2.4	11.9
SBA-15-U3	670	0.87	0.15	8.9	8.8	2.9	11.7
SBA-15-U4	525	0.42	0.19	5.8	5.4	5.2	10.6
SBA-15-U1-SH1	546	0.87	0.10	8.6	8.8	2.5	11.3
SBA-15-U1-SH2	334	0.42	0.09	6.0	6.2	3.8	10.0
SBA-15-DS1	909	1.18	0.16	8.7	9.2	2.3	11.5
SBA-15-DS2	958	1.16	0.22	7.4	7.8	2.5	10.3
SBA-15-DS3	952	0.88	0.22	5.6	6.9	2.8	9.7
SBA-15-DS4	935	0.99	0.21	5.2	7.0	2.3	9.3

[a] S_{BET}, BET specific surface area; V_t, single-point pore volume; V_c, volume of interconnecting pores of the diameter below 4 nm; w_{KJS}, mesopore diameter calculated by the KJS method (Kruk et al., 1997); w_d, mesopore diameter calculated on the basis of the unit cell parameter and pore volumes according to the relation derived for the hexagonal *P6mm* structure (Kruk et al., 1999) assuming 2.0 g/cm^3 density of silica; b, pore wall thickness; a, unit cell calculated from the observed chracteristic Bragg's reflection (100).

The unit cell parameters for the samples studied are summarized in Table 3. As can be seen from Fig. 2A, the diffraction profile for the extracted ureidopropyl-functionalized SBA-15-U1 silica exhibits one sharp reflection at $2\theta \sim 0.75$ indexed as (100) and two minor reflections (110) and (200); this pattern resemblances that for a purely siliceous SBA-15 (*P6mm* symmetry group). The XRD patterns for the remaining samples of this series (Panel A) were also analyzed according to the *P6mm* symmetry group. The XRD study shows that an increase in the concentration of ureidopropyl ligands (SBA-15-U4) meaningfully affected the XRD profiles, which is manifested by a reduction of the major and minor peak intensities suggesting a gradual deterioration of the mesostructural ordering. Analogous changes in the structural behavior were observed for bi-functional silicas (Fig. 2B) and bridged silicas (Fig. 2C). In all cases the major peaks showed a tendency to shift towards higher values of 2θ angles suggesting a slight decrease in the unit cell (see Table 3).

Pore structure characterization

Shown in Fig. 2 are nitrogen adsorption-desorption isotherms measured at $-196^{\circ}C$ (Panels D, E and F) and pore size distributions (Panels G, H and I) for the extracted SBA-15 silicas with various ureidopropyl, ureidopropyl-mercaptopropyl and disulfide groups. The PSD curves were calculated according to the KJS method (Kruk et al., 1997), which was established for the cylindrical pore geometry. The nitrogen adsorption isotherms measured were used to obtain the BET specific surface area (Brunauer et al., 1938), the volume of complementary pores, the single-point pore volume (Sing et al., 1985), the mesopore channel diameter and pore-wall thickness, which are summarized in Table 3. For the purpose of comparison, nitrogen adsorption isotherms measured on calcined SBA-15 samples are also shown. In general, all materials synthesized with the lowest content of all types of organic groups exhibit type IV adsorption-desorption isotherms. They have sharp capillary condensation steps, which reflect capillary condensation of adsorbate in uniform mesopore channels, and evaporation steps related to the evacuation of adsorbate from these pores. It is noteworthy that the lack of coincidence between adsorption and desorption branches of the isotherm generates a hysteresis loop, which for the aforementioned isotherms exhibits H1 type according to the IUPAC classification. In addition, the steeper capillary condensation branch is, the narrower the pore size distribution is observed. As can be seen in Panels D, E and F of Fig. 2 the position of capillary condensation step is shifting towards the smaller values of the relative pressure with increasing content of the introduced functionalities, which reflects a gradual reduction of the diameter of mesopore channels (see Panels

G, H and I in Fig. 2). For the SBA-15-U4, SBA-15-U1-SH2 and SBA-15-DS4 samples with the highest concentration of organics, the mesopore KJS diameters (see Table 3) were 5.8, 6.0 and 5.2 nm, respectively, whereas the PSDs were still narrow except that for SBA-15-U4, which was broad. Not only the KJS pore size, but also other adsorption parameters such as the BET specific surface area and single-point pore volume decreased with increasing content of organics. In the case of ureidopropyl-functionalized and bifunctional SBA-15 materials, the BET surface area was reduced from 866 m^2/g (calcined SBA-15) to 525 m^2/g for ureidopropyl-modified SBA-15 and to 334 m^2/g for bifunctional SBA-15, whereas the total pore volume was reduced from 1.38 cm^3/g to 0.42 cm^3/g (for both types of surface groups). As far as the disulfide groups incorporated into the silica framework, the BET surface area and the total pore volume almost did not change; even a slight increase was observed in the case of the BET surface area. This behavior is associated with the nature and structure of periodic mesoporous organosilicas because they possess bridging groups instead of surface ligands. However, it needs to be kept in mind that the content of bridging groups in this case was slightly lower in comparison to the content of surface ligands in the samples studied. In addition, for all SBA-15 silicas the pore wall thickness increased with increasing concentrations of U, U1-SH, DS groups and its highest value was obtained for materials modified with ureidopropyl surface ligands.

The information about complementary porosity of the functionalized silicas was assessed on the basis of PSDs; the volumes of complementary small pores are listed in Table 3. It is noteworthy that these fine pores are originated from the penetration of hydrophilic ethylene oxide blocks (EO) into the silica walls. Among the organosilicas studied the relatively high volumes of these pores were obtained for silica with disulfide bridging groups (see Panel I and Table 3), which can be due to the fact that the silica walls containing these organic spacers favor interactions with ethylene oxide blocks (EO). Moreover, these materials (DS2, DS3 and DS4) exhibit some higher fractions of textural pores, which are evidenced by the lack of plateau at higher pressures. In addition, desorption for SBA-15-DS2 and the samples with higher content of bridging groups tend to be much broader that reflects non-uniformity of pore openings.

3.2 Mesoporous cage-like SBA-16 organosilicas

Similarly to the SBA-15 organosilicas, elemental analysis was used to evaluate the introduction of surface and bridging groups into cage-like mesoporous SBA-16 silicas templated by block copolymer F127; the values of nitrogen and sulfur percentages as well as the estimated group coverages are listed in Table 2. These values are progressively increasing with increasing concentrations of incorporated groups.

The TG patterns and the corresponding differential TG (DTG) profiles for ureidopropyl-functionalized SBA-16 silicas (Panels A and D), ureidopropyl-mercaptopropyl-functionalized SBA-16 silicas (Panels B and E) and bis(propyl)disulfide-modified SBA-16 (Panel C and F) recorded under nitrogen atmosphere are displayed in Fig. 3, respectively. The TG study shows that the extraction of the block copolymer F127 template from cage-like SBA-16 organosilicas with acidified ethanol solution was incomplete. This is especially visible on the DTG curve for the first sample (SBA-16-U1) in the series of silicas containing ureidopropyl groups when compared with the corresponding DTG curve for the template-containing SBA-16-U1-t sample (see Fig. 3D). As can be seen from this figure the thermogravimetric event at $\sim$400°C for the extracted SBA-16-U1 sample, which is related to the decomposition of the F127 template, is still quite visible; it is possible that this sample has smaller pore openings. For the remaining ureidopropyl samples the extraction process was much better. However, it should be noted that the removal of polymeric templates from cage-like mesostructures is more difficult than in the case of channel-like mesostructures, especially when the cage openings in the former structures are small and the attached surface groups are relatively large.

Structural identification

The extracted cage-like SBA-16 samples were studied by powder X-ray diffraction. The XRD profiles for ureidopropyl-functionalized SBA-16, ureidopropyl-mercaptopropyl-functionalized SBA-16 and SBA-16 with disulfide bridging groups are shown in Fig. 4 (Panels A, B and C, respectively). The unit cell parameters are listed in Table 4. As can be seen from Fig. 4, the diffraction patterns for extracted functionalized SBA-16 materials exhibit a strong reflection at $2\theta \sim 0.8$ and

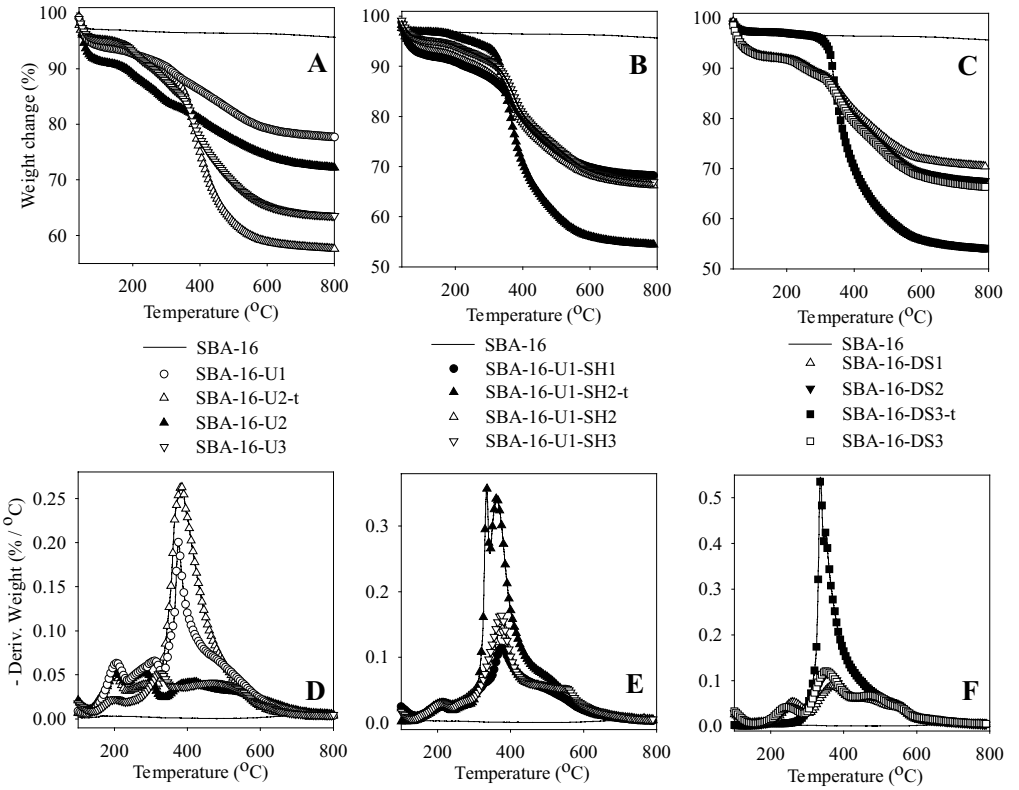

Fig. 3 High-resolution TG profiles (top panels) and the corresponding DTG profiles (bottom panels) recorded in flowing nitrogen for cage-like SBA-16 mesoporous silicas obtained via co-condensation using various concentrations of ureidopropyl (U) surface ligands (A, D), bifunctional surface ligands: ureidopropyl (U) and mercaptopropyl (SH) (B, E) and bis(propyl)disulfide (DS) bridging groups (C, F), respectively

some less-resolved minor reflections. The XRD profiles for these samples were assigned according to the cubic *Im3m* symmetry group (body-centered-packing) and thus the reflections were indexed as (110), (200) and (211). The major and minor peaks show a tendency to decrease with increasing concentration of introduced organic groups in SBA-16. For instance, a high concentration of ureidopropyl groups in the SBA-15-U4 sample caused a significant reduction in the intensity of major and minor XRD peaks in comparison to those observed for the SBA-16 samples with small amount of surface groups. This change in the XRD profile suggests visible structure deterioration in the samples with high concentrations of surface groups. Analogous structural changes were observed for bifunctional SBA-16 silicas (Fig. 4B) and the SBA-16 samples with bridging groups (Fig. 4C). Similarly to SBA-15, the position of the major peak for the DS-modified SBA-16 sample is offset towards higher values of 2θ suggesting a slight reduction in the unit cell (see Table 4).

Pore structure characterization

Nitrogen adsorption-desorption isotherms measured at -196°C for extracted SBA-16 silicas containing different amounts of ureidopropyl, ureidopropyl-mercaptopropyl surface groups and disulfide bridging groups are shown in Fig. 4 (Panels D, E and F, respectively). These isotherms were used to evaluate the following adsorption parameters: the BET specific surface area (Brunauer et al., 1938), single-point pore volume (Sing et al., 1985), mesopore diameter and pore wall thickness, which are listed in Table 4. Similarly to SBA-15, these panels show also nitrogen adsorption isotherms measured for calcined purely siliceous SBA-16 sample. The SBA-16 silicas with ureidopropyl groups and bi-functional samples with the smallest

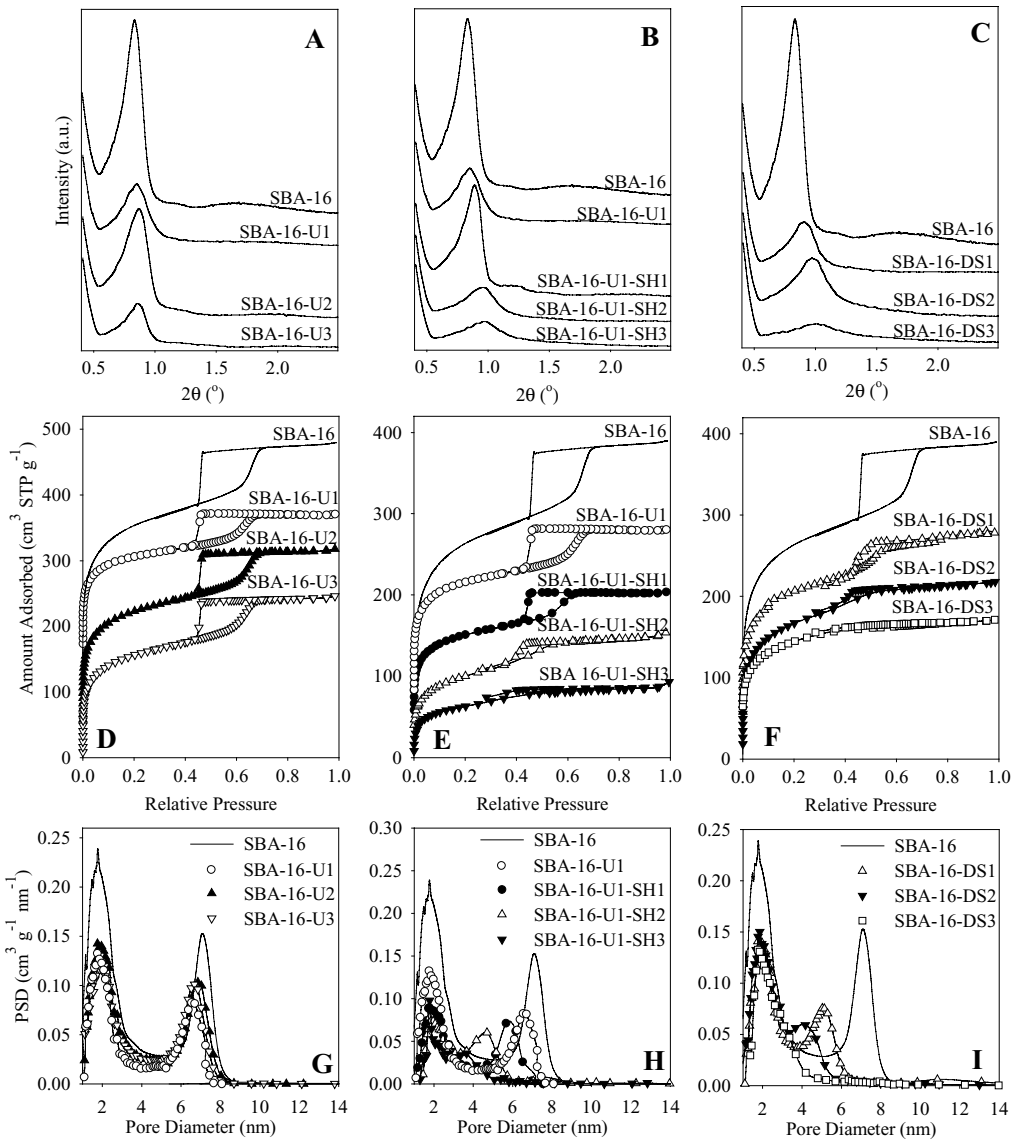

Fig. 4 X-ray diffraction (XRD) patterns (A, B, C), nitrogen adsorption isotherms (D, E, F) measured at –196°C and the corresponding pore size distributions (PSDs) (G, H, I) calculated according to the KJS method (Kruk et al., 1997) for the cage-like SBA-16 mesoporous silicas having various concentrations of ureidopropyl (U) surface ligands (A, D, G), bifunctional surface ligands; ureidopropyl (U) and mercaptopropyl (SH) (B, E, H) and bis(propyl)disulfide (DS) bridging groups (C, F, I), respectively. The isotherms in Panel D for SBA-16, SBA-16-U1 and SBA-16-U2 were offset vertically by 90, 165 and 50 cc STP g^{-1}. The isotherms in Panel E for SBA-16-U1 and SBA-16-U1-SH1 were offset vertically by 75 and 50 cc STP g^{-1}. The isotherms in Panel F for SBA-16-DS1 and SBA-16-U1-DS2 were offset vertically by 50 and 10 cc STP g^{-1}

concentration of these groups, SBA-16-U1 (Panel D) and SBA-16-U1-SH1 (Panel E), exhibit type IV adsorption-desorption isotherms with sharp capillary/evaporation steps and pronounced H2 hysteresis loops. The condensation step starts at a relative pressure of about 0.7, whereas the evaporation step ends suddenly at about 0.45, which is typical for mesoporous materials containing cage-like pores and narrow PSDs (see PSDs in Panels G and H). The value of relative pressure at which capillary evaporation takes place can be used to evaluate the size of pore openings. However, for the samples studied the hysteresis loops close at the limiting pressure value for nitrogen at −196°C, i.e., at relative pressure of about 0.45. In

Table 4 Selected structural parameters of the organic-functionalized cage-like SBA-16 mesoporous silicas[a]

Sample	S_{BET}, m^2g^{-1}	V_t, ccg^{-1}	V_c, ccg^{-1}	w_{KJS}, nm	w_d, nm	b, nm	a, nm
SBA-16	932	0.60	0.35	7.0	9.0	3.6	15.0
SBA-16-U1	494	0.32	0.18	6.5	8.1	4.4	14.8
SBA-16-U2	613	0.41	0.23	6.8	8.4	3.7	14.6
SBA-16-U3	553	0.38	0.20	6.7	8.5	3.6	14.7
SBA-16-U1-SH1	360	0.24	0.14	5.7	7.2	4.5	14.3
SBA-16-U1-SH2	357	0.20	0.09	4.7	7.0	4.4	13.2
SBA-16-U1-SH3	225	0.14	0.07	3.6	6.1	5.1	13.0
SBA-16-DS1	549	0.36	0.18	5.1	8.1	3.9	13.8
SBA-16-DS2	557	0.33	0.20	4.2	6.8	4.3	12.9
SBA-16-DS3	508	0.22	0.13	2.9	6.1	4.6	12.4

[a] $S_{BET,}$ BET specific surface area; V_t, single-point pore volume; V_c, volume of micropores and interconnecting pores of the diameter below 4 nm for SBA-16, SBA-16-U1, SBA-16-U2, SBA-16-U3, SBA-16-U1-SH1, whereas for other materials V_c was calculated below 3 nm; w_{KJS}, mesopore cage diameter calculated by the KJS method (Kruk et al., 1997); w_d, mesopore cage diameter calculated on the basis of the unit cell parameter and pore volumes according to the relation derived for the cubic *Im3m* structure (Kruk and Jaroniec, 2002) assuming 2.0 g/cm^3 density of silica; b, pore wall thickness; a, unit cell calculated from the observed chracteristic Bragg's reflection (110).

the case of disulfide-modified SBA-16 silicas (Panel F), the sample with lowest content of bridging groups (SBA-16-DS1) shows less steep capillary condensation and evaporation steps indicating broader PSD (Panel I) and larger non-uniformity of pore openings. As can be seen from Fig.s 4D, 4E and 4F, an increase in the concentration of organic groups reduces the steepness of the evaporation steps for bi-functional (Fig. 4E) and disulfide-modified SBA-16 silicas (Fig. 4F), which is not the case for U-functionalized materials (Fig. 4D). This example illustrates that the structural properties of cage-like materials are quite sensitive on the type of surface and bridging groups as well as their concentration. For instance, an increase in the concentration of U-SH and DS groups shifts the position of capillary condensation step towards lower values of relative pressure indicating a gradual reduction in the mesopore size (see PSDs in Figs. 4H and 4I, respectively). It is worth to mention that pore size distributions shown in Fig. 4 (G, H and I) were obtained by using the KJS method (Kruk et al., 1997) calibrated on the basis of adsorption data for channel-like mesopores with diameter between 2 and 6.5 nm. Since this calibration was done using MCM-41 materials with cylindrical pores, this method leads to the underestimation of the diameter of cage-like mesopores by about 2–3 nm. Therefore, Table 4 lists also the pore diameters calculated using geometrical relation between the pore volumes and the unit cell derived for cubic *Im3m* symmetry group (Kruk and Jaroniec, 2002).

Similarly to SBA-15-type organosilicas, adsorption parameters such as the BET surface area and single-point pore volume for the SBA-16-type organosilica samples decrease with increasing concentration of organic groups, except the SBA-16-U1 sample, which possesses some residue of the template. In the case of U-decorated SBA-16, bi-functional SBA-16 and DS-functionalized SBA-16, the BET surface area decreased from 932 m^2/g (calcined SBA-16) to 553 m^2/g, 225 m^2/g and 508 m^2/g, respectively, whereas the total pore volume decreased from 0.6 cm^3/g to 0.38 cm^3/g, 0.14 cm^3/g and 0.22 cm^3/g, respectively. Note that for DS-functionalized SBA-15 an opposite trend was observed. Furthermore, the thickness of mesopore walls shows a tendency to increase with increasing concentrations of U, U1-SH, DS groups.

As can be seen from PSDs in Fig. 4 (all panels), all functionalized silicas show larger volumes of complementary pores in relation to the volume of ordered pores, which can be calculated by subtracting the former from the total pore volume (see Table 4). It is interesting to notice that the relation between the volumes of complementary and ordered pores in SBA-15 is opposite because for this channel-like material the volume of ordered mesopores is large. However, the triblock copolymer F127 used to synthesize SBA-16 possesses 5.3 times more hydrophilic ethylene oxide blocks (EO) than the P123 polymer used to obtain SBA-15; therefore, for functionalized SBA-16 silicas the penetration

of EO blocks into pore walls can be more extensive than in the case of SBA-15. Also, in the case of cage-like materials the complementary porosity includes small ordered pores that interconnect large ordered cages.

4 Conclusions

Comparative studies of mesoporous materials of hexagonal (SBA-15) and cubic (SBA-16) symmetry with increasing concentrations of ureidopropyl surface groups, ureidopropyl and mercaptopropyl surface groups and bridging disulfide groups have been prepared by co-condensation of proper organosilanes and TEOS in the presence of poly(ethylene oxide)-*block*-poly(propylene oxide)-*block*-poly(ethylene oxide) triblock copolymers Pluronic P123 ($EO_{20}PO_{70}EO_{20}$) and Pluronic F127 ($EO_{106}PO_{70}EO_{106}$) as structure directing agents. It is shown that in the case of channel-like SBA-15 organosilicas the P123 template can be removed completely by extraction with hydrochloric acid-ethanol solution. In contrast, the removal of the F127 template from cage-like SBA-16 organosilicas was in some cases more difficult. The incorporation of various surface ligands and disulfide bridging group into SBA-15 and SBA-16 mesostructures was relatively successful. Both functionalized mesoporous channel-like and cage-like silicas showed long-range crystallographic ordering that was reduced systematically with increasing concentration of the introduced functionality. All cage-like SBA-16 organosilicas showed higher volume ratio of complementary pores to ordered mesopores in comparison to that observed for channel-like SBA-15 silicas. In contrast to the SBA-15 organosilicas, the SBA-16 organosilicas with higher contents of functional groups tended to have smaller volume of mesopores. This study shows that the incorporation of various surface and bridging groups into cage-like mesostructures is more difficult than in the case of channel-like mesostructures, for which this incorporation can be performed without significant diminishment of the pore volume and surface area. Since the aforementioned functionalized mesoporous organosilicas possess high affinity toward metal ions such as mercury, lead and cadmium there are promising adsorbents for removal of these pollutants from aqueous solutions.

Nomenclature

a	unit cell parameter (nm)
b	pore wall thickness (nm)
S_{BET}	BET specific surface area (m^2/g)
V_c	volume of micropores and interconnecting pores of the diameter below 4 nm for SBA-15 and SBA-16, (cc/g)
V_t	single-point pore volume (cc/g)
w_d	mesopore diameter calculated on the basis of the unit cell parameter and pore volumes according to equations 1 and 2 derived for the cubic and hexagonal structures, respectively (nm)
w_{KJS}	mesopore diameter at the maximum of pore size distribution calculated by the KJS method (nm)

Acknowledgment M.J. acknowledges support by the National Science Foundation Grant CTS-0553014. Thanks to undergraduate student Donald J. Knobloch from Saint Vincent College, Latrobe, PA 15650, USA, participant of the NSF-supported REU program (grant CHE-0353737) at the Chemistry Department of Kent State University during summer 2005 for assistance in some experiments reported in this paper.

References

Abu-Lebdeh, Y.A.I., P.M. Budd, and V.M. Nace, *J. Mater. Chem.*, **8**, 1839 (1998).

Antochshuk, V. and M. Jaroniec, *Chem. Commun.*, 2373–2374 (1999).

Antochshuk, V. and M. Jaroniec, *Chem. Mater.*, **12**, 2496 (2000).

Antochshuk, V. and M. Jaroniec, *J. Phys. Chem. B*, **103**, 6252 (1999).

Antochshuk, V., O. Olkhovyk, M. Jaroniec, I.-S. Park, and R. Ryoo, *Langmuir*, **19**, 3031 (2003).

Asefa, T., M.J. MacLachlan, N. Coombos, and G.A. Ozin, *Nature*, **402**, 867 (1999).

Bao, X.Y., X.S. Zhao, X. Li, P.A. Chia, and J. Li, *J. Phys. Chem. B*, **108**, 4684 (2004).

Barrett, E.P., L.G. Joyner, and P.H. Halenda, *J. Am. Chem. Soc.*, **73**, 373 (1951).

Beck, J.S., J.C. Vartuli, W.J. Roth, M.E. Leonowicz, C.T. Kresge, K.D. Schmitt, C.T.-W. Chu, D.H. Olson, E.W. Sheppard, S.B. McCullen, J.B. Higgins, and J.L. Schlenker, *J. Am. Chem. Soc.*, **114**, 10843 (1992).

Brunauer, S., P.H. Emmet, and E. Teller, *J. Am. Chem. Soc.*, **60**, 309 (1938).

Corriu, R.J.P., A. Mehdi, C. Reye, and C. Thieulux, *Chem. Commun.*, 1382 (2002).

Feng, X., G.E. Fryxell, L.Q. Wang, A.Y. Kim, J. Liu, and K. Kemmer, *Science*, **276**, 923 (1997).

Fiorilli, S., B. Ondia, B. Bonelli, and E. Garrone, *J. Phys. Chem. B*, **109**, 16725 (2005).
Fowler, C.E., S.L. Burkett, and S. Mann, *Chem. Commun.*, 1769 (1997).
Gierszal, K.P., T.-W. Kim, R. Ryoo, and M. Jaroniec, *J. Phys. Chem. B*, **109**, 23263 (2005).
Gong, Y.J., Z.H. Li, D. Wu, Y.H. Sun, F. Deng, Q. Luo, and Y. Yue, *Microporous Mesoporous Mater.*, **49**, 95 (2001).
Grudzien, R.M. and M. Jaroniec, *Chem. Commun.*, 1076 (2005).
Grudzien, R.M., B.E. Grabicka, and M. Jaroniec, *J. Mater. Chem.*, **16**, 819 (2006).
Grudzien, R.M., B.E. Grabicka, M. Kozak, S. Pikus, and M. Jaroniec, *New J. Chem.*, **30**, 1071 (2006).
Grudzien, R.M., B.E. Grabicka, S. Pikus, and M. Jaroniec, *Chem. Mater.*, **18**, 1722 (2006).
Grudzien, R.M., B.E. Grabicka, D.J. Knobloch, and M. Jaroniec, *Colloids and Surfaces A*, **291**, 139 (2006).
Grudzien, R.M., S. Pikus, and M. Jaroniec, *J. Phys. Chem. B*, **110**, 2972 (2006).
Hamoudi, S. and S. Kaliaguine, *Microporous Mesoporous Mater.*, **59**, 195 (2003).
Hatton, B., K. Landskron, W. Whitnall, D. Perovic, and G.A. Ozin, *Acc.Chem. Res.*, **38**, 305 (2005).
Hodgkins, R.P., A.E. Garcia-Bennett, and P.A. Wright, *Microporus and Mesoporous Mater.*, **79**, 241 (2005).
Huh, S., J.W. Wiench, J.-Ch. Yoo, M. Pruski, and V.S.-Y. Lin, *Chem. Mater.*, **15**, 4247 (2003).
Inagaki, S., S. Guan, T. Ohsuna, and O. Teraski, *Nature*, **416**, 204 (2002).
Inagaki, S., S. Guan, Y. Fukushima, T. Ohsuna, and O. Teresaki, *J. Am. Chem. Soc.*, **121**, 9611 (1999).
Jaroniec, M, *Nature*, **442**, 638 (2006).
Jaroniec, C.P., M. Kruk, M. Jaroniec, and A. Sayari, *J. Phys. Chem. B*, **102**, 5503 (1998).
Kang, T., Y. Park, K. Choi, J.S. Lee, and J. Yi, *J. Mater. Chem.*, **14**, 1043 (2004).
Kao, H.M., J.-D. Wu, Ch.-Ch. Cheng, and A.S.T. Chiang, *Microporous Mesoporous Mater.*, **88**, 319 (2006).
Kim, T.-W., R. Ryoo, M. Kruk, K.P. Gierszal, M. Jaroniec, S. Kamiya, and O. Teresaki, *J. Phys. Chem. B*, **108**, 11480 (2004).
Kresge, C.T., M.E. Leonowicz, W.J. Roth, J.C. Vartuli, and J.S. Beck, *Nature*, **359**, 710 (1992).
Kruk, M. and M. Jaroniec, *Langmuir*, **18**, 844 (2002).
Kruk, M., E.B. Celer, and M. Jaroniec, *Chem. Mater.*, **16**, 698 (2004).
Kruk, M., M. Jaroniec, and A. Sayari, *Langmuir*, **13**, 6267 (1997).
Kruk, M., M. Jaroniec, and A. Sayari, *Chem. Mater.*, **11**, 492 (1999).
Kruk, M., M. Jaroniec, C.H. Ko, and R. Ryoo, *Chem. Mater.*, **12**, 1961 (2000).
Kruk, M., M. Jaroniec, Y. Sakamoto, O. Terasaki, R. Ryoo, and Ch.H. Ko, *J. Phys. Chem. B*, **104**, 292 (2000).
Kruk, M., V. Antochshuk, J.R. Matos, L.P. Mercuri, and M. Jaroniec, *J. Am. Chem. Soc.*, **124**, 168 (2002).
Kruk, M., T. Asefa, N. Coombs, M. Jaroniec, and A.G. Ozin, *J. Mater. Chem.*, **12**, 3452 (2002).
Kuroki, M., T. Asefa, W. Whitnal, M. Kruk, C. Yoshina-Ishii, M. Jaroniec, and G.A. Ozin, *J. Am. Chem. Soc.*, **124**, 13886 (2002).
Liang, Y., M. Hanzlik, and R. Anwander, *J. Mater. Chem.*, **15**, 3919 (2005).
Lim, M.H. and A. Stein, *Chem. Mater.*, **11**, 3285 (1999).
Lim, M.H., C.F. Blanford, and A. Stein, *J. Am. Chem. Soc.*, **119**, 4090 (1997).
Liu, J., J. Yang, Q. Yang, G. Wang, and Y. Li, *Adv. Funct. Mater.*, **15**, 1297 (2005).
Matos, J.R., M. Kruk, L.P. Mercuri, M. Jaroniec, L. Zhao, T. Kamiyama, O. Teresaki, T.J. Pinnavaia, and Y. Liu, *J. Am. Chem. Soc.*, **125**, 821 (2003).
Matos, J.R., M. Kruk. L.P. Mercuri, M. Jaroniec, T. Asefa, N. Coombos, G. A. Ozin, and O. Teresaki, *Chem. Mater.*, **14**, 1903 (2002).
Melde, B.J., B.T. Holland, C.F. Blandford, and A. Stein, *Chem. Mater.*, **11**, 3302 (1999).
Olkhovyk, O. and M. Jaroniec, *Adsorption*, **11**, 205 (2005).
Olkhovyk, O. and M. Jaroniec, *J. Am. Chem. Soc.*, **127**, 60 (2005).
Olkhovyk, O., S. Pikus, and M. Jaroniec, *J. Mater. Chem.*, **15**, 1517 (2005).
Olkhovyk, O., V. Antochshuk, and M. Jaroniec, *Colloids and Surfaces A*, **236**, 67 (2004).
Sakamoto, Y., M. Kaneda, O. Teresaki, D. Zhao, J.M. Kim, G. Stucky, H.J. Shin, and R. Ryoo, *Nature*, **408**, 449 (2000).
Sing, K.S.W., D.H. Everett, R.A.W. Haul, L. Moscou, R.A. Pierotti, J. Rouquerol, and T. Siemieniewska, *Pure Appl. Chem.*, **57**, 603 (1985).
Srivastava, R., D. Srinivas, and P. Ratnasamy, *Microporous Mesoporous Mater.*, **90**, 314 (2006).
Stein, A., *Adv. Mater.*, **15**, 763 (2003).
Stein, A., B.J. Melde, and R.C. Schroden, *Adv. Mater.*, 1**2**, 1403 (2000).
Tanev, P.T. and T.J. Pinnavaia, *Science*, **267**, 865 (1995).
Tanev, P.T., M. Chibwem, and T.J. Pinnavaia, *Nature*, **368**, 321 (1994).
Voort, P.V.D., M. Benjelloun,, and E.F. Vansant, *J. Phys. Chem. B*, **106**, 9027 (2002).
Wang, L., J. Fan, B. Tian, H. Yang, Ch. Yu, B. Tu, and D. Zhao, *Microporous Mesoporous Mater.*, **67**, 135 (2004).
Wang, X., K.S.K. Lin, J.C.C. Chan, and S. Cheng, *J. Phys. B*, **109**, 1763 (2005).
Wang, Y.Q., C.M. Yang, B. Zibrowius, B. Spliethoff, M. Linden, and F. Schuth, *Chem. Mater.*, **15**, 5029 (2003).
Wei, Q., Z. Nie, Y. Hao, Z. Chen, J. Zou, and W. Wang, *Mater. Lette.*, **59**, 3611 (2005).
Yanagisawa, T., T. Shimizu, K. Kuroda, and C. Kato, *Bull. Chem. Soc. Japan*, **63**, 988 (1990).
Yang, Ch.-M., Y. Wang, B. Zibrowius, and F. Schuth, *Phys. Chem. Chem. Phys.*, **6**, 2461 (2004).
Yang, P., D. Zhao, D.I. Margolese, B.F. Chmelka, and Stucky, *Chem. Mater.*, **11**, 2813 (1999).
Yu, C., Y. Yu, and D. Zhao, *Chem. Commun.*, 575 (2000).
Zapilko, C. and R. Anwander, *Chem. Mater.*, **18**, 1479 (2006).
Zhang, F., Y. Yan, H. Yang, Y. Meng, Ch. Yu, B. Tu, and D. Zhao, *J. Phys. Chem. B*, **109**, 8723 (2005).
Zhang, L., W. Zhang, J. shi, Z. Hua, Y. Li, and J. Yan, Chem. *Commun.*, 210 (2003).
Zhao, D., Q. Huo, J. Feng, B.F. Chmelka, and G.D. Stucky. *J. Am. Chem. Soc.*, **120**, 6024 (1998).
Zhao, L., G. Zhu, D. Zhang, Y. Di, O. Teresaki, and Sh. Qiu, *J. Phys. Chem. B*, **109**, 764 (2004).